Appl. Phys. A (2016) 122:303
DOI 10.1007/s00339-016-9788-1

Applied Physics A
Materials Science & Processing

Bioactivity of fluorapatite/alumina composite coatings deposited on Ti6Al4V substrates by laser cladding

C. S. Chien[1,2] · C. W. Liu[3] · T. Y. Kuo[3] · C. C. Wu[3] · T. F. Hong[4]

Received: 8 October 2015 / Accepted: 19 October 2015 / Published online: 7 March 2016

Abstract Hydroxyapatite (HA) is one of the most commonly used coating materials for metal implants. However, following high-temperature deposition, HA easily decomposes into an unstable phase or forms an amorphous phase, and hence, the long-term stability of the implant is reduced. Accordingly, the present study investigates the use of fluorapatite (FA) fortified with 20 wt% alumina (α-Al_2O_3) as an alternative biomedical coating material. The coatings are deposited on Ti6Al4V substrates using a Nd:YAG laser cladding process performed with laser powers and travel speeds of 400 W/200 mm/min, 800 W/400 mm/min and 1200 W/600 mm/min, respectively. The results show that for all of the specimens, a strong metallurgical bond is formed at the interface between the coating layer and the transition layer due to melting and diffusion. The XRD analysis results reveal that the cladding layers in all of the specimens consist mainly of FA, β-TCP, CaF_2, Ti and θ-Al_2O_3 phases. In addition, the cladding layers of the specimens prepared using laser powers of 400 and 800 W also contain $CaTiO_3$ and $CaAl_2O_4$, while that of the specimen clad using a power of 1200 W contains TTCP and CaO. Following immersion in simulated body fluid for 14 days, all of the specimens precipitate dense bone-like apatite and exhibit excellent bioactivity. However, among all of the specimens, the specimen that is prepared with a laser power of 800 W shows the best biological activity due to the presence of residual FA, apatite-generating $CaTiO_3$ and a rough cladding layer surface.

✉ T. Y. Kuo
tykuo@mail.stust.edu.tw

[1] Department of Orthopaedics, Chimei Foundation Hospital, Tainan 710, Taiwan, ROC

[2] Department of Electrical Engineering, Southern Taiwan University of Science and Technology, Tainan 710, Taiwan, ROC

[3] Department of Mechanical Engineering, Southern Taiwan University of Science and Technology, Tainan 710, Taiwan, ROC

[4] Graduate Institute of Materials Engineering, National Pingtung University of Science and Technology, Pingtung 912, Taiwan, ROC

1 Introduction

Titanium and its alloys have high strength, light weight and excellent corrosion resistance. Moreover, their elastic modulus is closer to human bone than that of other metallic biomaterials such as SUS 304L stainless steel and CoCrMo alloys. Consequently, the stress shielding effect with natural bone is lower, and hence, the risk of implant loosening and bone re-fracturing is reduced. As a result, titanium alloys are one of the most widely used commercial metallic implant materials. However, such metals are bioinert and therefore do not readily form chemical bonds with the host tissue. As a result, the implants tend to become detached from the tissue following long-term implantation. It has been shown that the mechanical properties and biological activities of biomedical implants can be enhanced by coating the implant with a bioceramic material, such as TiO_2, AW glass and hydroxyapatite (HA, $Ca_{10}(PO_4)_6OH_2$). Among these materials, HA has a Ca/P ratio similar to that of natural bone [1] and has particularly good biocompatibility and osteoconduction properties [2–6]. It is thus currently the most widely used commercial coating material for metallic implants. However, following high-temperature coating processes, such as plasma spraying, HA tends to decompose and form unstable phase. Consequently, the long-term stability of the implant is degraded. Moreover, if a low-temperature coating process is used (e.g., sol–gel processing), the bonding

strength between the coating material and the substrate is reduced, and hence, the long-term survivability of the implant is once again adversely affected.

Fluorapatite (FA, $Ca_{10}(PO_4)_6F_2$) has the same apatite phase as HA and shares a similar composition. Moreover, compared to HA, FA has a higher interatomic bonding strength, an improved chemical stability, a lower dissolution rate, a better thermal stability and a reduced bioresorption rate [7–12]. As a result, FA has many theoretical advantages for implant applications. However, plasma-sprayed coatings containing FA alone commonly exhibit micro-cracks and voids on the coating surface and have weak mechanical properties [13]. It has been shown that for HA coatings, the addition of reinforcing agents such as zirconia (ZrO_2) and alumina (Al_2O_3) reduces the thermal expansion coefficient mismatch between the coating and the substrate and improves the mechanical properties and biological performance as a result [14–17]. Thus, the addition of reinforcing agents to FA has also attracted growing attention in recent years.

Among the various ceramic reinforcements available, Al_2O_3 is one of the most widely used materials for orthopedic applications due to its excellent wear resistance [9]. Furthermore, Al_2O_3 is both thermally stable and chemically inert. Previous studies have shown that the bonding strength of sintered HA/Al_2O_3 composite samples increases with an increasing Al_2O_3 content [17]. In addition, it has been shown that Al_2O_3 has excellent biocompatibility, mechanical strength, fatigue resistance and corrosion resistance [18, 19]. It is thus one of the most frequently used materials for total hip and knee replacements and many other implant applications [20].

Many studies have shown that laser cladding enhances the bonding strength between bioceramic materials such as HA and FA and metallic substrates and hence inhibits the disintegration and detachment of the coating layer [21–25]. In a previous study [22], the present group investigated the effects of TiO_2 addition on the surface microstructure and bioactivity of FA coatings deposited on Ti6Al4V substrates using an Nd:YAG laser. In the present study, an investigation is performed into the bonding interface, phase composition and bioactivity properties of Al_2O_3-reinforced FA coatings deposited on Ti6Al4V substrates using a Nd:YAG laser cladding process with a constant laser power/travel speed (*P*/*V*) ratio of 2:1 and three different settings of the laser power and travel speed, namely 400 W/200 mm/min, 800 W/400 mm/min and 1200 W/600 mm/min.

2 Experiments

The cladding trials were performed using Ti6Al4V alloy plates with dimensions of 100 mm × 60 mm × 3 mm, and the chemical composition is given in Table 1. The FA

Table 1 Chemical composition (wt%) of Ti–6Al–4V

Al	V	O	Fe	C	N	H	Ti
6.1	4.24	0.152	0.16	0.017	0.008	0.0006	Balance

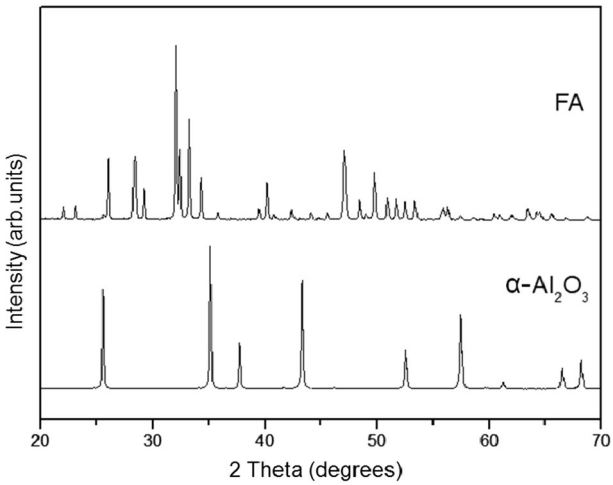

Fig. 1 XRD patterns of coating powders: **a** FA and **b** α-Al_2O_3

powder was prepared via a solid-state reaction of $3Ca_3(PO_4)_2 + CaF_2 \rightarrow Ca_{10}(PO_4)_6F_2$ [26] using $Ca_3(PO_4)_2$ (β-TCP, β-tricalcium phosphate) and CaF_2 (Sigma-Aldrich, USA) as the starting powders. Briefly, the powders were mixed and milled in a stoichiometric molar ratio of 3:1 with ZrO_2 balls in ethanol for 48 h. After drying, the mixed powders were compacted and heated at 1000 °C for 3 h in air to form solid FA cylinders. The FA powder was fortified using 20 wt% Al_2O_3 alumina (α-Al_2O_3) (Sigma-Aldrich, USA). The atomic structures of the FA powder and Al_2O_3 powder were examined using XRD (Fig. 1). The FA powder and Al_2O_3 alumina were mixed with a polyvinyl alcohol binder material ($(C_2H_4O)_n$) in a 3:1 ratio (wt%) and then thoroughly stirred until a slurry-like consistency was obtained. The slurry was pre-placed on the substrate surface to form a coating layer with a thickness of approximately 0.8 mm and was then dried in an oven at 100 °C for 30 min under atmospheric conditions. Finally, the specimens were laser-clad using an Nd:YAG laser (ROFIN CW025, 2500 W; Rofin Sinar Technologies Inc., Germany) set to a continuous-wave operation mode. The cladding trials were performed using a constant laser power/travel speed (*P*/*V*) ratio of 2:1. However, to clarify the effect of the laser power on the metallurgical and bioactivity properties of the samples, three different combinations of the cladding parameters were considered, namely 400 W/200 mm/min, 800 W/400 mm/min and 1200 W/600 mm/min. The laser beam was guided to the workstation by an optical fiber with a core diameter of

600 μm and was focused to a spot size diameter of approximately 3 mm by a lens with a focal length of 120 mm. The cladding process was performed in an Ar-shielded atmosphere (Ar flow rate: 25 l/min) with a 5° laser incident angle and a 15-mm plus defocus length. The experimental setup is shown in Fig. 2.

The microstructures of the clad specimens were observed using SEM (JEOL JSM-6390LV, JEOL Ltd., Japan). Following SEM inspection, the specimens were cleaned, sterilized and immersed in a standard simulated body fluid (SBF) solution prepared in accordance with Kokubo's protocol [27]. The ion concentrations in the SBF solution and human blood plasma, respectively, are presented in Table 2. The specimens were soaked for 2, 7 and 14 days at a temperature of 37 ± 0.1 °C and were then examined for the nucleation and growth of apatite using SEM and EDS. In addition, the phases within the coatings

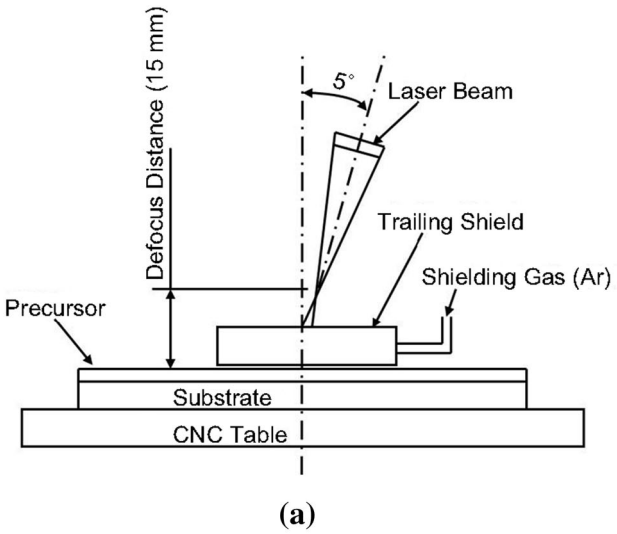

Fig. 2 **a** Schematic illustration of Nd-YAG laser cladding process and **b** photograph of experimental setup

Table 2 Inorganic ion concentrations of SBF and human blood plasma

(mM)	Na^+	K^+	Ca^{+2}	Mg^{+2}	Cl^-	HCO_3^-	HPO_4^{-2}
SBF	142.0	5.0	2.5	1.5	148.8	4.2	1.0
Blood	142.0	5.0	2.5	1.5	103.0	27.0	1.0

were identified using XRD (Cu Kα radiation, Rigaku D/Max Ⅲ.V, Rigaku Ltd., Japan) with a 2θ scanning range of 20°–70° and a scanning rate of 2° min^{-1}.

3 Results and discussion

3.1 Morphology and microstructure of weld beads

Figure 3 presents SEM images of the coating layer (CL) and transition layer (TL) in each of the laser-clad samples. It is seen that the microstructural morphologies of the three samples are very similar despite the difference in laser power. Furthermore, it is observed that for each specimen, the CL structure is loosely organized, while the TL structure is more dense. The lower SEM images in Fig. 3 show that all of the CL microstructures contain globular particles. Figure 4a presents an SEM image of the CL in the sample prepared using a laser power of 1200 W. Figure 4b, c shows the EDS analysis results for globular particles A and B in Fig. 4a. Figure 4b shows that particle A consists mainly of Ti and P. The presence of TiP compounds (Ti phosphides) [11] suggests a partial thermal decomposition of the FA content in the CL during the high-temperature cladding process accompanied by a thermal-induced melting and diffusion of Ti from the substrate. As the laser power increases, the extent of FA decomposition and Ti melting/diffusion also increases, and hence, Ti phosphides of a greater size are formed, as shown in Fig. 3. It is noted that the present results are consistent with those of Ye et al. [11], which showed that a large number of Ti phosphides (Ti_xP_y) were formed when sintering Ti/FA (1:1) composite powders under temperatures of 1100 or 1200 °C. However, Ti phosphides can have a wide range of compositions, and it is thus difficult to reliably determine the exact composition of Ti_xP_y by XRD data alone [28]. Notably, the EDS results presented in Fig. 4c, corresponding to particle B in Fig. 4a, show that even under the maximum laser power (1200 W), the CL matrix still contains a large amount of fluoride. In other words, the potential for FA residue or conversion into fluoride still exists even under high cladding temperatures, as discussed later in Sect. 3.3.

Figure 5 presents the EDS line scan results for the individual alloying elements of the cladding layer near the CL/TL interface of the specimen prepared using a laser

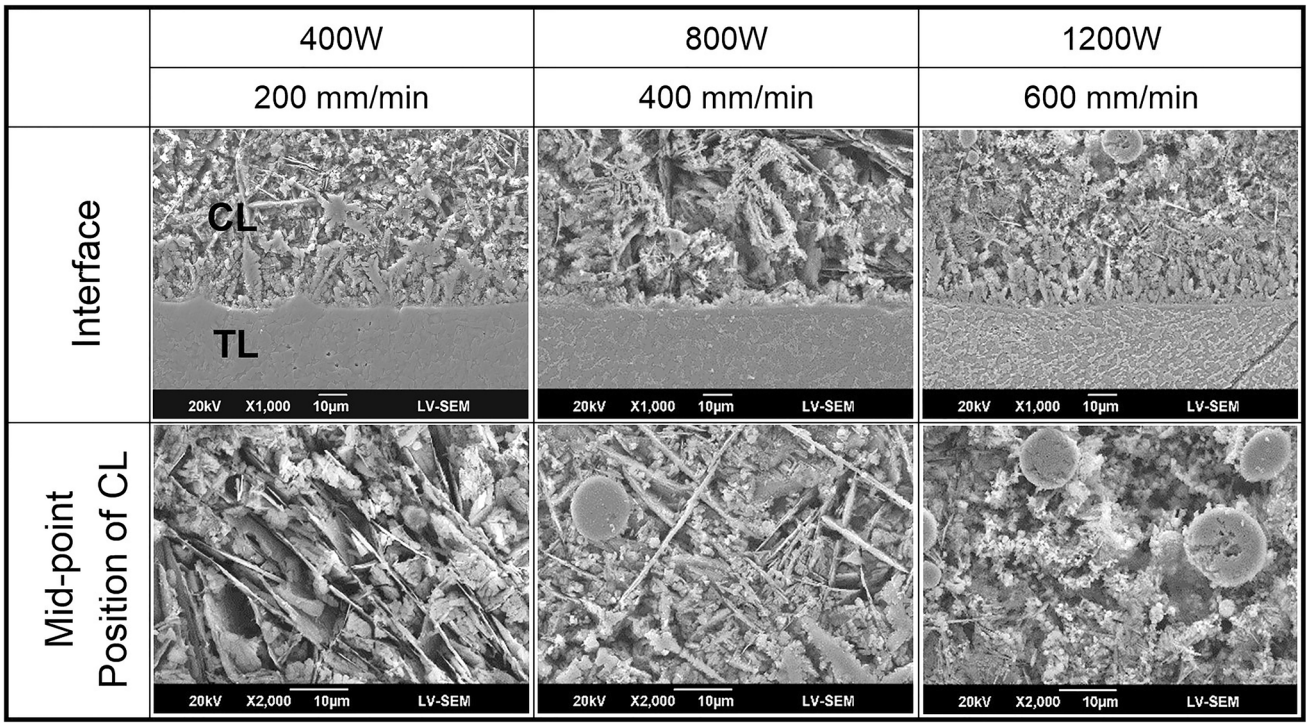

Fig. 3 SEM metallographs of CL/TL interface and midpoint position of CL in FA/Al_2O_3 specimens prepared using different laser cladding parameters. *Note* CL denotes coating layer and TL denotes transition layer

power of 1200 W. It is seen that the Ca and F elements, i.e., the main decomposition components of FA, are confined almost entirely to the CL. It has been reported that in the thermal decomposition of FA, F is either vaporized as HF gas or forms fluoride [9]. Thus, the F content in the CL layer most probably comes from the FA or fluoride, but must be analyzed by XRD for confirmation (see Sects. 3.2, 3.3). The P and O ions in the coating material have the ability to diffuse rapidly from the CL to the TL due to their small radii and low activation energy. Nonetheless, as shown in Fig. 5, some ions still remain within the CL. It is noted, however, that some of the P ions produced in the FA decomposition process simply vaporize in the high-temperature cladding process [21, 22]. Observing the results presented in Fig. 5, it is seen that the distributions of Al in the CL and TL, respectively, are roughly the same. In other words, given an addition of 20 wt% Al_2O_3 to the FA cladding material, a certain amount of Al remains within the CL despite the high-temperature diffusion effect.

3.2 In vitro bioactivity of laser-clad coatings

Figure 6 shows the surface morphologies of the FA/Al_2O_3 coatings before and after immersion in SBF. Among the as-prepared samples, the specimen prepared using a laser power of 800 W has the greatest surface roughness, followed by that prepared using a power of 1200 W. In other words, for a constant *P*/*V* ratio, the surface morphology is not directly related to the laser power. Following immersion in SBF for 3 days, all of the specimens show evidence of bone-like apatite growth. The apatite growth is particularly dense in the case of the specimen prepared with a laser power of 800 W. After 7 days, all of the specimens show an increased apatite growth. Notably, dense apatite structures are observed not only on the specimen clad with a laser power of 800 W, but also on that prepared with a power of 400 W. Following the maximum immersion time of 14 days, dense apatite is also formed on the surface of the sample clad with a laser power of 1200 W. Overall, the images suggest that the samples prepared using low and medium laser powers (i.e., 400 and 800 W) have better biological activity than that prepared with a high laser power (i.e., 1200 W). As discussed in Sect. 3.3, this suggests that low and medium laser powers lead to a greater residual FA within the CL and a greater nucleation of apatite via $CaTiO_3$ phase [29]. The CL of the 800 W specimen has a qualitatively rougher surface than the 400 W specimen. Thus, the surface offers a better environment for apatite growth, and hence, the rate of apatite formation is enhanced. Notably, the presence of $CaTiO_3$ in the CL not only prompts the nucleation of apatite, but also improves the bonding strength between the apatite and the substrate [30, 31].

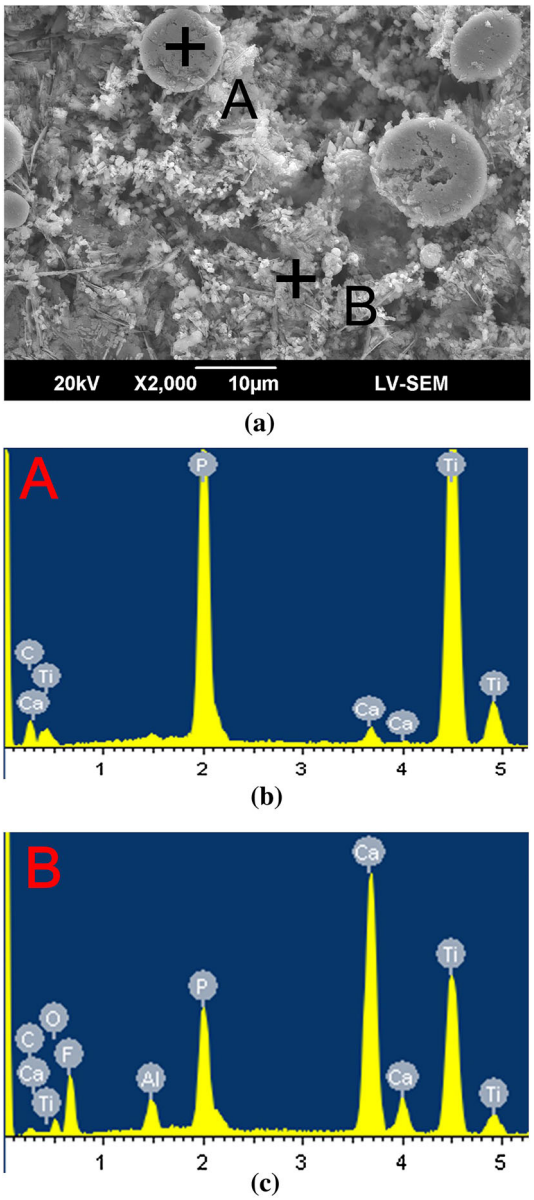

Fig. 4 SEM and EDS analyses of CL microstructure in specimen prepared using laser parameters of $P = 1200$ W and $V = 600$ mm/min: **a** SEM metallograph of midpoint position of CL, **b** EDS results for *point A* in **a** and **c** EDS results for *point B* in **a**

3.3 XRD patterns of CL surface before and after SBF immersion

Figure 7 shows the XRD patterns of the various specimens before and after SBF immersion. It is seen that prior to immersion (day 0), the CLs of the 400 and 800 W specimens consist mainly of FA, β-TCP, CaF_2, Ti, θ-Al_2O_3, $CaTiO_3$ and $CaAl_2O_4$. For the 1200 W specimen, the CL has no $CaTiO_3$ or $CaAl_2O_4$ phase, but contains tetracalcium phosphate [TTCP, $Ca_4(PO_4)_2O$] phase and a large quantity of CaO. Previous studies have shown that CaF_2 phase is produced in the decomposition of FA even under relatively low sintering temperatures [32]. However, at higher temperatures (above 1100 °C), the CaF_2 transforms to CaO through hydrolysis [i.e., $CaF_2 + H_2O \rightarrow CaO + 2HF_{(g)}$] [9, 11]. Thus, the high CaO content in the CL of the present specimen prepared using a laser power of 1200 W is most likely due to the thermally induced hydrolysis of CaF_2.

It has been reported that FA and Al_2O_3 react to produce TCP and $CaAl_2O_4$ ($Ca_{10}(PO_4)_6F_{2(s)} + Al_2O_{3(s)} + H_2O_{(g)} \rightarrow 3Ca_3(PO_4)_{2(s)} + CaAl_2O_{4(s)} + 2HF_{(g)}$) at high-temperature process [9]. Moreover, in the present samples, the formation of $CaTiO_3$ phase occurs due to the reaction between Ca (decomposed from FA) and Ti from the Ti6Al4V substrate. The presence of $CaAl_2O_4$ can also be attributed to a solid reaction between Al_2O_3 and CaO [9]. However, the TTCP most likely arises from FA phase transition under high-temperature conditions. The P/V ratio for the 1200 W specimen is the same as that for the 400 W and 800 W specimens (i.e., 2:1). However, due to the higher power rate, the specimen receives a greater energy density, and hence, the degree of FA decomposition is enhanced. The XRD spectra of the as-prepared samples show that under a high energy density, the tendency of the FA phase to transit to TTCP is greater than its tendency to react with the substrate to form $CaTiO_3$ (reason yet to be confirmed). In addition, θ-Al_2O_3 is a transformation from original α-Al_2O_3 power.

Following SBF immersion for 3 days, most of the peaks in the original XRD spectra are reduced or disappear. Moreover, a weak HA peak begins to emerge. As the immersion time increases, the intensity of the HA peak also increases. After soaking for 14 days, all of the specimens exhibit a strong HA peak, indicating the dense growth of HA on the specimen surface. The 800 W specimen exhibits the strongest HA peak followed by the 400 W specimen. In other words, the XRD results for the HA tendency are consistent with the SEM images shown in Fig. 6.

In a thermal decomposition process, apatite decomposes first to β-TCP, and β-TCP then gradually transforms to α-TCP and TTCP as the temperature increases [33]. As commented above, the laser cladding process performed in this study is a high energy density process. Given a sufficiently high laser power (e.g., 1200 W), the heating effect causes the coating material to decompose and form TTCP and CaO, or other high-temperature phases. Notably, CaO is a bioinert phase and thus reduces the biocompatibility of the coating [24]. FA has a higher-temperature stability than HA [7, 34]. However, under high laser powers, FA decomposition is unavoidable and the formation of TTCP and bioinert CaO phase cannot be prevented. The mechanical properties of TCP and TTCP are poorer than those of FA. Furthermore, TCP and TTCP both biodegrade more rapidly than FA. Consequently, the 1200 W

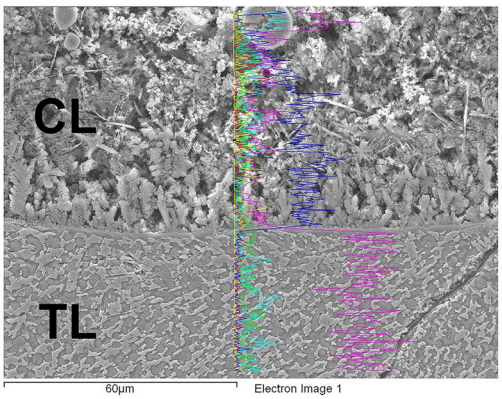
CL
TL
60µm
Electron Image 1

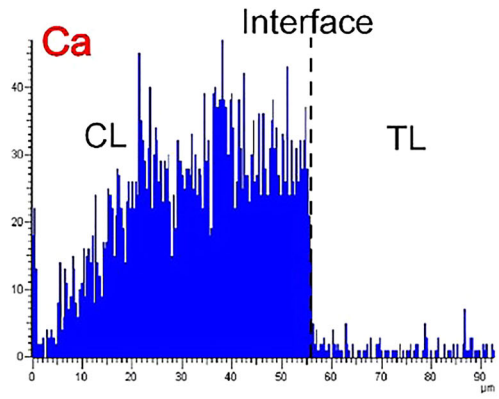
Ca
Interface
CL
TL
µm

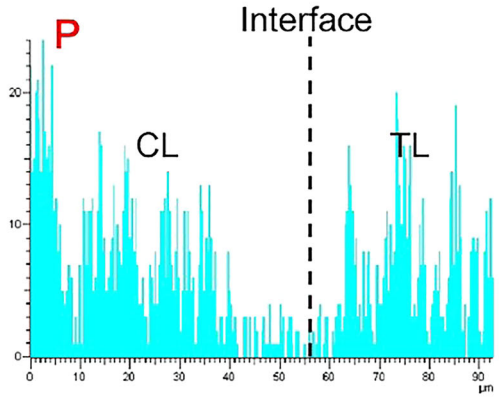
P
Interface
CL
TL
µm

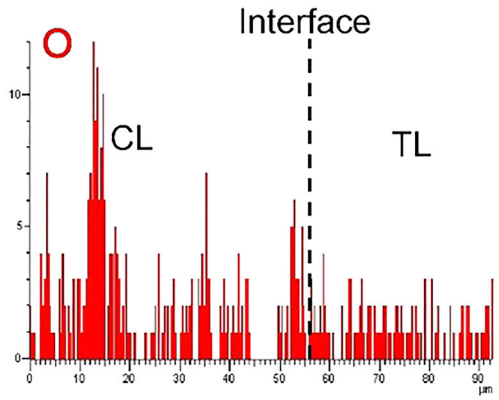
O
Interface
CL
TL
µm

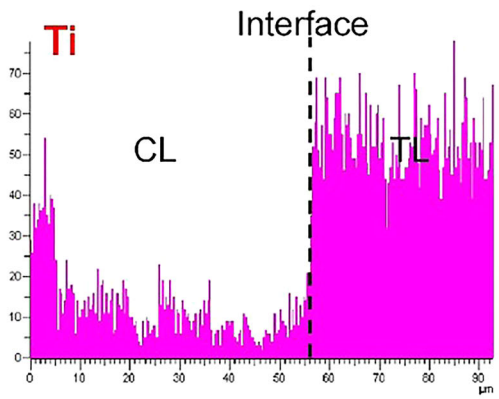
Ti
Interface
CL
TL
µm

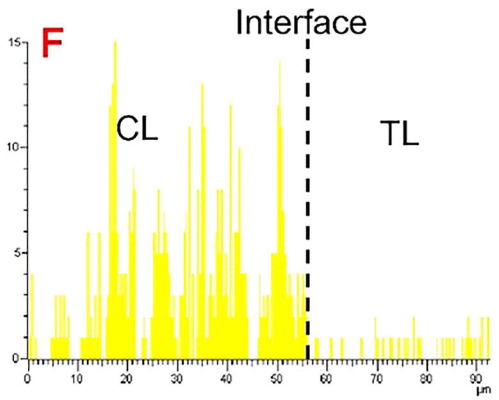
F
Interface
CL
TL
µm

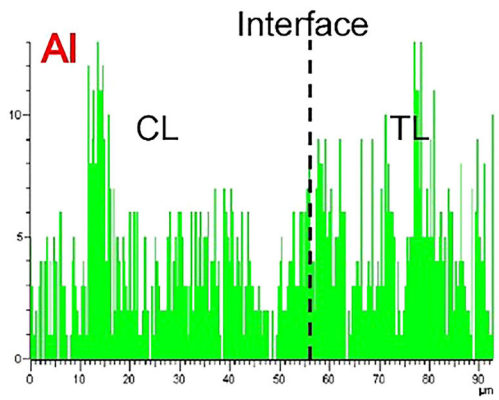
Al
Interface
CL
TL
µm

◀**Fig. 5** EDS line scans showing Ca, P, O, Ti, F and Al contents in CL and TL regions of FA/Al_2O_3 coating prepared using laser parameters of $P = 1200$ W and $V = 600$ mm/min

specimen, with a higher TTCP and CaO content, exhibits the poorest bioactivity of the present samples.

3.4 Micro-hardness evaluation

Figure 8 shows the cross-sectional hardness profiles of the various laser-clad samples. It is observed that the hardness of the TL is significantly greater than that of the substrate in all three samples. However, the CL hardness is only slightly higher than that of the substrate. For all specimens, only a moderate variation in the CL–TL-substrate (shown sequentially from left to right) hardness occurs, and hence, a superior interface bonding performance is obtained. From inspection, the hardness of the CL in the three samples has a value in the range of 1000–1300 HV, with the 800 W specimen having the highest hardness, followed by the 400 W specimen. In other words, the hardness and the power rate are not directly related. It is noted, however,

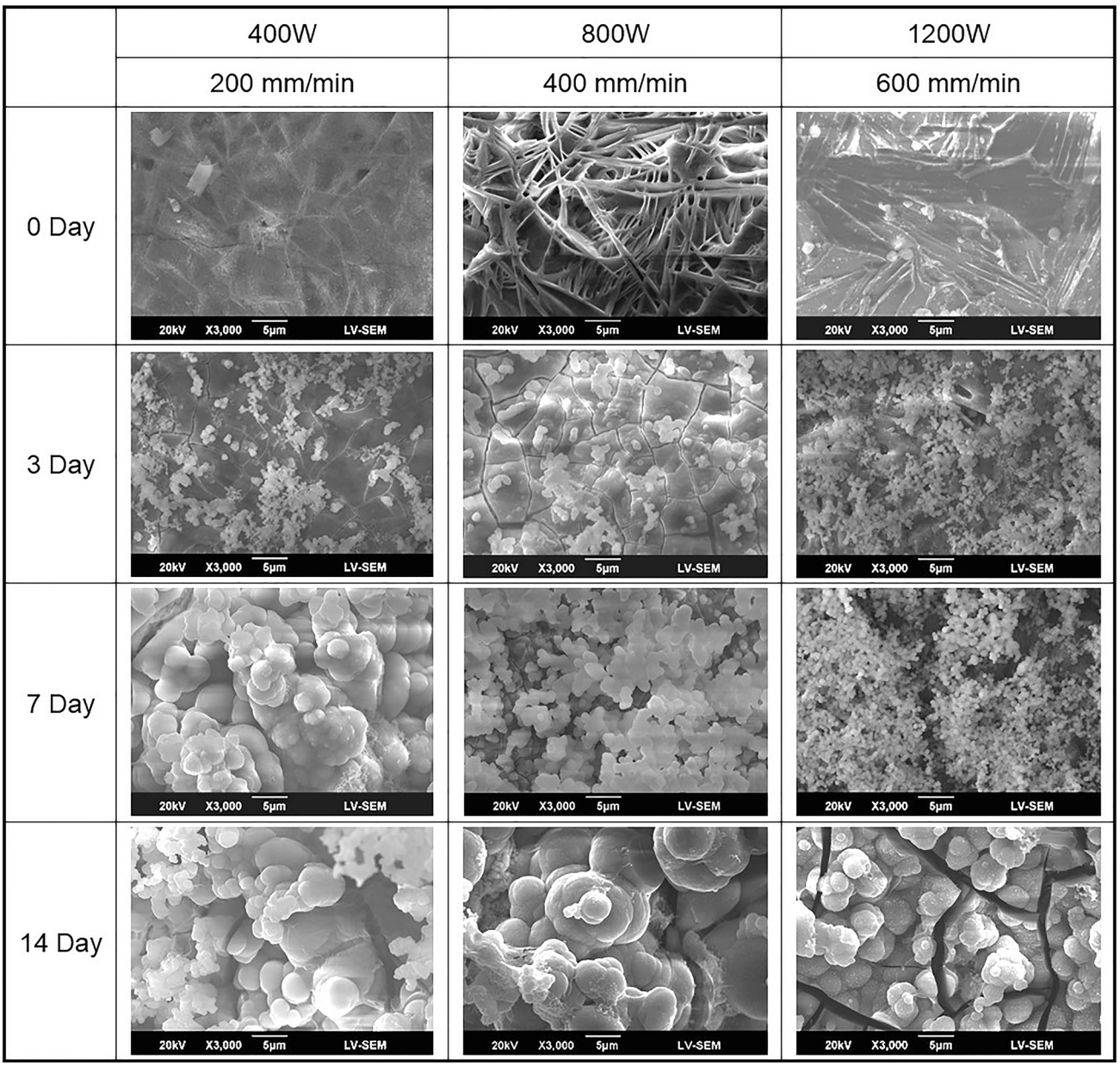

Fig. 6 SEM images showing CL surface of FA/Al_2O_3 specimens following immersion in SBF for periods of 0–14 days. **a** 400 W, **b** 800 W, **c** 1200 W

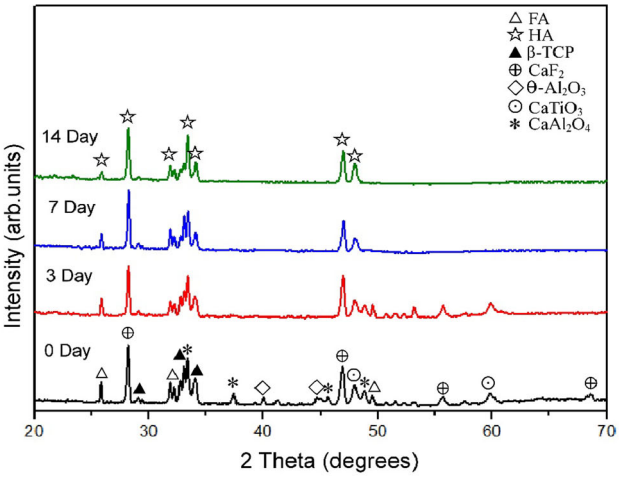

(a) 400W

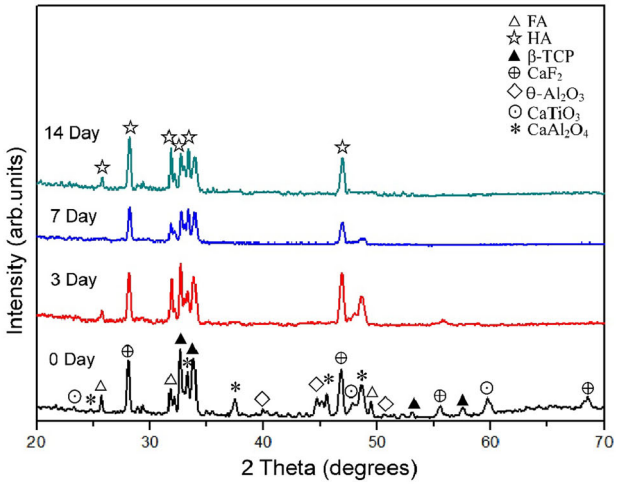

(b) 800W

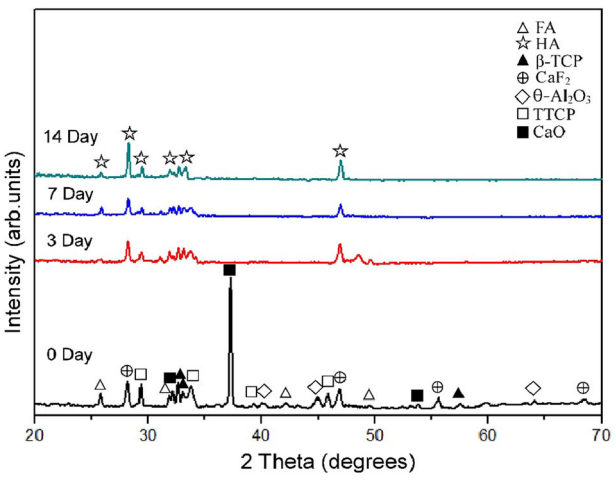

(c) 1200W

◀**Fig. 7** XRD analysis results for CLs of specimens before and after SBF immersion

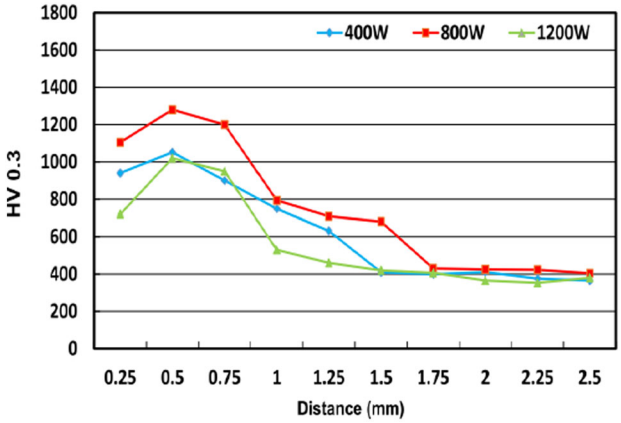

Fig. 8 Cross-sectional hardness profiles of FA/Al_2O_3 specimens

that the power rate is significantly related to the generation of calcium aluminate phase ($CaAl_2O_4$).

Previous studies [14, 35, 36] have shown that adding Al_2O_3 powder to HA via sintering at temperatures in the range of 1200–1400 °C results in an increased hardness. Furthermore, under a higher sintering temperature, a more severe HA decomposition occurs, and hence, a greater amount of calcium aluminate phases (such as $CaAl_2O_4$, $Ca_3Al_2O_6$ and $Ca_5Al_6O_{14}$) are formed. Calcium aluminates act as a hard phase and thus constrain the shrinkage of the matrix as well as their own densification [14]. As a result, the mechanical strength increases. Juang and Hon [36] suggested that the densification of the sintered products and the formation of calcium aluminate phases after sintering are the main factors accounting for the enhanced hardness and strength of HA with Al_2O_3 reinforcement.

In this study, partial thermal decomposition of the FA occurs due to the high-temperature cladding process. The resulting TCP, TTCP and CaO phases are more biodegradable than FA, and hence, the mechanical properties of the CL are reduced. However, the $CaAl_2O_4$ phase [9] formed through the reaction of TCP and CaO with Al_2O_3 (the reinforcing agent) inhibits the reduction in the mechanical properties [17] and thus performs a complementary role. Among the three specimens, the CLs in the 400 W and 800 W specimens both contain $CaAl_2O_4$ and therefore have a higher hardness than the 1200 W specimen. Moreover, the 800 W specimen has a greater $CaAl_2O_4$ content than the 400 W specimen (see Fig. 7a, b) and thus has a higher hardness.

HA, FA and Al_2O_3 are all bioceramics and have hardness higher than that of Ti alloy. However, their exact hardness values vary depending on the particular coating

technique used and the parameter settings applied. For example, recent studies have shown that their hardness may range from 260 to 1000 HV [21, 37–39]. The results obtained in this study have shown that the addition of Al_2O_3 to FA yields a hardness value of up to 1300 HV. The hardness is clearly related to the type and structure of the compounds formed in the coating layer. However, the available information does not relate hardness to the quality of the coating [39].

4 Conclusions

FA coatings fortified with 20 wt% alumina (Al_2O_3) have been deposited on Ti6Al4V substrates using a Nd:YAG laser cladding process with laser powers/travel speeds of 400 W/200 mm/min, 800 W/400 mm/min and 1200 W/600 mm/min, respectively. The experimental results support the following major conclusions.

1. Given a constant laser power/travel speed (*P*/*V*) ratio, a higher laser power does not prompt any significant change in the cladding layer (CL) or transition layer (CL) microstructure. However, globular Ti phosphides are formed in greater quantities within the CL as the laser power increases. For all samples, significant element diffusion occurs across the coating/substrate interface and thus results in a good metallurgical bonding strength.
2. The XRD analysis results have shown that the CL in all of the samples consists mainly of FA, β-TCP, CaF_2, Ti and Al_2O_3. In addition, the samples prepared using laser powers of 400 and 800 W contain $CaTiO_3$ and $CaAl_2O_4$ phases, while that prepared using a laser power of 1200 W contains TTCP and CaO.
3. Given the same laser *P*/*V* ratio, the specimen prepared using a laser power of 800 W contains apatite-generating $CaTiO_3$, a rougher CL surface and a residual amount of FA. As a result, it has the best bioactivity of the various samples. Overall, the results show that the laser cladding of FA/Al_2O_3 results in excellent bioactivity.
4. The CL hardness of the present specimens reaches a maximum value of 1300 HV (800 W specimen). The hardness can be attributed to the reinforcement effect provided by the $CaAl_2O_4$ phase. For all specimens, only a moderate variation in the CL–TL-substrate hardness occurs, and hence, a superior interface bonding performance is obtained.

Acknowledgments The authors gratefully acknowledge the financial support provided to this research by the Chimei Foundation Hospital, Republic of China (Taiwan), under Grant Number 110990223, and the Ministry of Science and Technology of the Republic of China (Taiwan) under Grant Number NSC 101-2221-E-218-017.

References

1. V.P. Orlovskii, V.S. Komlev, S.M. Barinov, Hydroxyapatite and hydroxyapatite-based ceramics. Inorg. Mater. **38**(10), 973–984 (2002)
2. J. Venkatesan, S.K. Kim, Chitosan composites for bone tissue engineering—an overview. Mar. Drugs **8**(8), 2252–2266 (2010)
3. A. Oryan, S. Alidadi, A. Moshiri, N. Maffulli, Bone regenerative medicine: classic options, novel strategies, and future directions. J. Orthop. Surg. Res. **9**(18), 1–27 (2014)
4. S.D. Cook, K.A. Thomas, J.F. Kay, M. Jarcho, Hydroxyapatite-coated titanium for orthopedic implant applications. Clin. Orthop. Relat. Res. **232**, 225–243 (1988)
5. S.M. Besta, A.E. Porterb, E.S. Thian, J. Huang, Bioceramics: past, present and for the future. J. Eur. Ceram. Soc. **28**(7), 1319–1327 (2008)
6. K. Kuroda, M. Okido, Hydroxyapatite coating of titanium implants using hydroprocessing and evaluation of their osteoconductivity. Bioinorg. Chem. Appl. **2012**, 1–7 (2012)
7. Y. Chen, X. Mian, Thermal and chemical stability of fluorohydroxyapatite ceramics with different fluorine contents. Biomaterials **26**(11), 1205–1210 (2005)
8. H.R. Rawls, B.F. Zimmerman, Fluoride-exchanging resins for caries for caries protection. Caries Res. **17**(1), 32–43 (1983)
9. F.B. Ayed, J. Bouaziz, Sintering of tricalcium phosphate–fluorapatite composites by addition of alumina. Ceram. Int. **34**(8), 1885–1892 (2008)
10. K.A. Bhadang, K.A. Gross, Influence of fluorapatite on the properties of thermally sprayed hydroxyapatite coatings. Biomaterials **25**(20), 4935–4945 (2004)
11. H. Ye, X.Y. Liu, H. Hong, Fabrication of titanium/fluorapatite composites and in vitro behavior in simulated body fluid. J. Mater. Sci. Technol. **29**(6), 523–532 (2013)
12. J. Weng, X. Liu, X. Zhang, X. Ji, Thermal decomposition of hydroxyapatite structure induced by titanium and its dioxide. J. Mater. Sci. Lett. **13**(3), 159–161 (1994)
13. M.H. Fathi, E.M. Zahrani, A. Zomorodian, Novel fluorapatite/niobium composite coating for metallic human body implants. Mater. Lett. **63**(13–14), 1195–1198 (2009)
14. B. Viswanath, N. Ravishankar, Interfacial reactions in hydroxyapatite/alumina nanocomposites. Scr. Mater. **55**(10), 863–866 (2006)
15. W. Suchanek, M. Yoshimura, Processing and properties of hydroxyapatite-based biomaterials for use as hard tissue replacement implants. J. Mater. Res. **13**(1), 94–117 (1998)
16. S. Gautier, E. Champion, D. Bernache-Assollant, Processing, microstructure and toughness of Al_2O_3 platelet-reinforced hydroxyapatite. J. Eur. Ceram. Soc. **17**(11), 1361–1369 (1997)
17. J. Li, B. Fartash, L. Hermansson, Hydroxyapatite—alumina composites and bone-bonding. Biomaterials **16**(5), 417–422 (1995)
18. G. Heimke, S. Leyen, G. Willmann, Knee arthoplasty: recently developed ceramic offer new solutions. Biomaterials **23**(7), 1539–1551 (2002)
19. A. Ignatius, M. Perous, S. Schorlemmer, P. Augat, W. Burger, S. Leyen, L. Claes, Osseointergration of alumina with a bioactive coating under load-bearing and unloaded conditions. Biomaterials **26**(15), 2325–2332 (2005)
20. M. Hamadouche, L. Sedel, Ceramics in orthopaedics. J. Bone Joint Surg. Br. **82**(8), 1095–1099 (2000)

21. C.S. Chien, T.Y. Liao, T.F. Hong, T.Y. Kuo, C.H. Chang, M.L. Yeh, T.M. Lee, Surface microstructure and bioactivity of hydroxyapatite and fluorapatite coatings deposited on Ti–6Al–4V substrates using Nd-YAG laser. J. Med. Biol. Eng. **34**(2), 109–115 (2014)
22. C.S. Chien, Y.S. Ke, T.Y. Kuo, T.Y. Liao, T.M. Lee, T.F. Hong, Effect of TiO_2 addition on surface microstructure and bioactivity of fluorapatite coatings deposited using Nd:YAG laser. Proc. Inst. Mech. Eng. H **228**(4), 379–387 (2014)
23. C.S. Chien, T.F. Hong, T.J. Han, T.Y. Kuo, T.Y. Liao, Effects of different binders on microstructure and phase composition of hydroxyapatite Nd–YAG laser clad coatings. Appl. Surf. Sci. **257**(6), 2387–2393 (2011)
24. D.G. Wang, C.Z. Chen, J. Ma, T. Lei, Microstructure of yttric calcium phosphate bioceramic coatings synthesized by laser cladding. Appl. Surf. Sci. **253**(8), 4016–4020 (2007)
25. G.J. Cheng, D. Pirzada, M. Cai, P. Mohanty, A. Bandyopadhyay, Bioceramic coating of hydroxyapatite on titanium substrate with Nd–YAG laser. Mater. Sci. Eng. C **25**(4), 541–547 (2005)
26. H.W. Kim, Y.M. Kong, Y.H. Koh, H.E. Kim, H.M. Kim, J.S. Ko, Pressureless sintering and mechanical and biological properties of fluor-hydroxyapatite composites with zirconia. J. Am. Ceram. Soc. **86**(12), 2019–2026 (2003)
27. T. Kokubo, H. Takadama, How useful is SBF in predicting in vivo bone bioactivity. Biomaterials **27**(15), 2907–2915 (2006)
28. C.Q. Ninga, Y. Zhoub, On the microstructure of biocomposites sintered from Ti, HA and bioactive glass. Biomaterials **25**(17), 3379–3387 (2004)
29. B.Y. Chou, E. Chang, Plasma-sprayed hydroxyapatite coating on titanium alloy with ZrO_2 second phase and ZrO_2 intermediate layer. Surf. Coat. Technol. **153**(1), 84–92 (2002)
30. Y. Ohba, T. Watanabe, E. Sakai, M. Daimon, Coating of Hap/$CaTiO_3$ multilayer on titanium substrates by hydrothermal method. J. Ceram. Soc. Jpn. **107**(10), 907–912 (1999)
31. S. Yin, Y. Fujishiro, S. Uchida, T. Sato, Characterization of ceria and yttria co-doped zirconia/alumina composites crystallized in supercritical methanol. J. Supercrit. Fluids **13**(1–3), 363–368 (1998)
32. F.B. Ayed, J. Bouaziz, K. Bouzouita, Calcination and sintering of fluorapatite under argon atmosphere. J. Alloys Compd. **322**(1–2), 238–245 (2001)
33. S.V. Dorozhkin, Calcium orthophosphate-based bioceramics. Materials. **6**(9), 3840–3942 (2013)
34. J.C. Elliott, *Structure and chemistry of the apatites and other calcium orthophosphates* (Elsevier Science B.V., The London Hospital Medical College, Department of Child Dental Health, London, 1994)
35. J.I. Huaxia, P.M. Marquis, Sintering behavior of hydroxyapatite with 20 wt% Al_2O_3. J. Mater. Sci. **28**(7), 1941–1945 (1993)
36. H.Y. Juang, M.H. Hon, Fabrication and mechanical properties of hydroxyapatite-alumina composites. Mater. Sci. Eng. C **2**(1–2), 77–81 (1994)
37. C.S. Chien, T.Y. Liao, T.F. Hong, T.Y. Kuo, J.L. Wu, T.M. Lee, Investigation into microstructural properties of fluorapatite Nd–YAG laser clad coatings with PVA and WG binders. Surf. Coat. Technol. **205**(10), 3141–3146 (2011)
38. C.S. Chien, T.J. Han, T.F. Hong, T.Y. Kuo, T.Y. Liao, Effects of different hydroxyapatite binders on morphology, Ca/P ratio and hardness of Nd–YAG laser clad coating. Mater. Trans. **50**(12), 2852–2857 (2009)
39. M. Tlotleng, E. Akinlabi, M. Shukla, S. Pityana, Microstructures, hardness and bioactivity of hydroxyapatite coatings deposited by direct laser melting process. Mater. Sci. Eng. C **43**, 189–198 (2014)